

# UAV Mobility Detection Using Radio Channel Properties for Collision Avoidance in Air Corridor

Wout Haak

**Abstract**—This paper discusses a UAV (Unmanned Aerial Vehicle) mobility detection scheme to realize the safe air mobility in air corridor. It is crucial for UAVs to detect the mobility of its neighboring UAVs in order to plan a trajectory in real time and avoid collisions. This paper focuses on the utilization of radio channel properties acquired from the transmit-receive antennas loaded on the UAV to detect its neighbor UAV's mobility. The UAVs of interest are quadcopter drones. From the scattered radio signals, the micro-Doppler frequency shift is extracted and contains information of the rotational velocity of the propellers. Moreover, the snapshot power delay profile contains real time information of the distance between the drones. The project is electromagnetic (EM) simulator based and the results show that the drone's orientation has an influence on the micro-Doppler signatures. To add on that, the obtained power delay profile, when using the cross-polarized pair of transmit-receive antennas, shows the drone's propellers instead of the drone's body. Based on these findings, a collision avoidance scheme is summarized.

**Index Terms**—Cross-polarized antennas, backscattered radio channel, rotary drone, air mobility, micro-Doppler effect, spectrogram, air corridor, collision avoidance.

## I. INTRODUCTION

Over the last few years, UAVs (Unmanned Aerial Vehicles) have increased in popularity. From quick deliveries to environmental monitoring, the features of the drones, largely due to the less congested air mobility, are proving to be extremely beneficial. More and more businesses realized its potential. For example the agriculture, aerial photography, package delivery businesses and the military sector have already adopted drone technology. NASA's vision for Advanced Air Mobility (AAM) is to help emerging aviation markets to safely develop an air transportation system that moves people and cargo between places previously not served by aviation [1]. In the prospected future, air mobility enabled by UAVs will be regulated in a dedicated air corridor. However, trajectory planning and collision avoidance of the UAVs are among the main research challenges. One of the promising solution is radio based technology, e.g. radar, in other words, the backscattering enabled radio sensing. Radio-based technology can be used for both sensing and communication applications, and is not influenced by lighting conditions.

In order to avoid the collisions in air corridor, the concerned UAV has to detect the mobility of other UAVs. There are many types of UAVs, this paper focuses on the quadcopter drone, since quadcopters are the most popular drone type on the market [2]. A quadcopter is a rotary drone consisting of four rotating propellers and a body frame. When a radar signal is transmitted to a rotary drone, it interacts with the drone and

returns back to the radar. The back-scattered signal contains information about the characteristics of the drone.

Relevant research mostly focuses on radar recognizing multi-propeller drones using micro-Doppler linear spectral pattern in long Doppler coherent processing interval circumstances [3]. The paper [3] focuses on the investigation of the influence of geometry design such as blade number, blade shape, drone's geometry and propeller synchronisation. These features are extracted from simulated micro-Doppler spectra and further processed in a support vector machine. Moreover, a paper [4] exploited the radar micro-Doppler signatures to discriminate birds and small UAVs. These micro-Doppler features are extracted using spectrograms and cepstrograms enabling automatic classification algorithms to make a distinction between man-made objects and bio-life.

The link between the air-to-air radio channel incorporating the UAV body frame/propeller and the collision avoidance has not been intensively studied. An investigation on safe air mobility could help emerging aviation markets to safely develop a safe air corridor in the near future. Therefore, the objective of this project is to detect the mobility of a rotary drone using radio channel properties in order to avoid collisions in air corridor.

The paper is EM simulator based and describes a method on how to obtain and exploit the radio channel function containing the transmitting, propagating, scattering and receiving radio wave information. In the simulator, two drones are modelled to emulate possible scenarios in the prospected air corridor. One drone is labeled as the 'observer' drone and the other drone the 'target' drone. The observer drone contains the transmit-receive antennas and sends out radar signals towards the target drone. Based on the radio channel information, the observer drone has to detect the mobility of the target drone in order to plan its trajectory and avoid collisions. To be feasible to accomplish the project within 10 weeks, the dual dynamic situation is simplified to a single dynamic situation.

The paper is structured as follows. Firstly, the methodology will be described in section II. Secondly, the numerical analysis and examples is explained in section III. Lastly, the paper will be concluded in section IV.

## II. METHODOLOGY

In this section, the methodology of the radio channel based UAV mobility detection is introduced. Firstly, the basic working principle of a drone will be described, this gives us insight in how propeller configurations relate to the drone's motion. Secondly, the micro-Doppler pattern of the backscattered radio channel will be modelled, this model

reveals the frequency dependence of the scattered radio waves caused by the rotational motion of the propeller. This section proposes a method that captures the micro-Doppler signatures as well as the delayed radio wave components that are scattered on a rotary drone. Lastly, based on the rotational velocity of the propellers and the range of the drone, collision avoidance will be discussed.

### A. Working principle of a quadcopter drone

The quadcopter is a type of rotary drone consisting of four electrical motors. When the drone is hovering, two opposing rotors are rotating clockwise and the other two counter-clockwise. This results in a net torque of zero acting on the drone, which makes the drone keep its orientation during flight. The spinning blades of the rotors push air down and since all forces come in pairs, the air pushes up the rotor [5]. When the net thrust of the rotors is larger than the gravitational force, the drone will experience a lift force. In case of hovering, the rotors excite a net thrust that equals the gravitational force. The load speed of the propellers depend on the drone type but most propellers on consumer drones spin at a rate of 8000 rpm which corresponds to a rotation rate of approximately 133 Hz [6].

In addition to translation movements, a drone in flight is free to rotate in three dimensions. These dimensions are the transverse, vertical and longitudinal axis or also called the pitch ( $\theta$ ), roll ( $\varphi$ ) and yaw ( $\psi$ ) axis. In Figure 1 the quadcopter as well as the aircraft principal axis is drawn.

1) *Pitch*: Pitch ( $\theta$ ) movement is the rotation of the aircraft about the y axis. For example, when rotor R2 and R3 are spinning faster than rotor R1 and R4, the drone will rotate in the positive pitch direction. As a consequence, the thrust force of the angled rotors can be decomposed in a horizontal force, providing a forward motion acting on the drone. The maximum pitch angle depends on the drone type, but for consumer drones, like the Phantom 4, it has a maximum pitch angle of around 40 degrees [7].

2) *Roll*: Roll ( $\varphi$ ) is the rotation about the x axis. The flying principle works the same as pitch movement since the quadcopter is symmetrical about the z axis. As depicted in Figure 1, if R1 and R2 are spinning faster than R3 and R4, the drone will rotate in the positive roll direction.

3) *Yaw*: Yaw ( $\psi$ ) is the rotation about the z axis. For example when the clockwise rotors R1 and R3 are rotating faster than the counter-clockwise rotors R2 and R4, there would be a net angular momentum acting on the drone, and therefore the drone will rotate clockwise.

### B. The micro-Doppler effect

The Doppler frequency shift is the change in frequency of the scattered radio waves when the target object is moving along the line of sight (LOS). The movement of the body of the drone for example will induce constant Doppler frequency shift. However, a rotary drone does not undergo one type of motion. The rotating motion of the propellers is called a micro-motion. The micro motion dynamics induces an additional

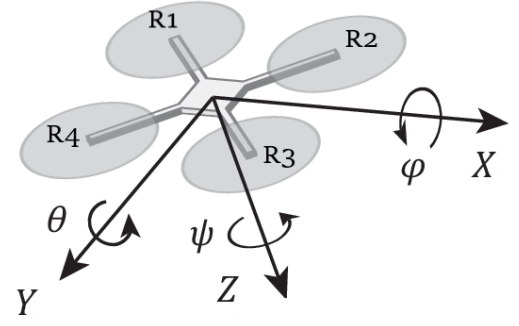


Fig. 1: Principal axis of a quadcopter [8]

Doppler frequency shift, called the micro-Doppler effect. The micro-Doppler effect in radar depends on the frequency of the radio wave and the relative velocity of the target object. The Doppler frequency shift can be calculated using the following equation [9]:

$$f_D = \frac{-2fv}{c_0} \quad (1)$$

where  $f$  is the frequency of the incoming radio waves,  $c_0$  the speed of light at which radio waves travel and  $v$  the relative velocity of the object along the LOS. The relative blade tip velocity along the LOS is expressed as  $v_{tip} = v_r \cos(2\pi\Omega t)$ , where  $v_r$  is tangential velocity,  $\Omega$  the rotation rate of the propeller and  $t$  the time [17]. When the propeller is perpendicular to the LOS, the highest tip velocity is reached and therefore induces the maximum Doppler shift. A positive Doppler frequency shift is caused by an approaching propeller blade and a negative shift is caused by a receding propeller blade.

According to the paper [10] a thin-wire model has been proposed to simulate the micro-Doppler patterns of the scattered radar signals. The model is simplified by modelling the blades of the propellers using thin wires. The synthetic scattered signal of the quadcopter can be described as:

$$\begin{aligned} E^{drone}(t, r_0) &\sim \sum_{p=1}^P E_p^{prop}(t, r_p, \theta_{p,b,w}, l_{p,b,w}) \\ &= \sum_{p=1}^P \sum_{b=1}^B \sum_{w=1}^W E_{p,b,w}^{wire}(t, r_p, \theta_{p,b,w}, l_{p,b,w}) \\ &= \sum_{p=1}^P \sum_{b=1}^B \sum_{w=1}^W \int_0^{l_{p,b,w}} j\eta \frac{k e^{-jkr_p}}{4\pi r_p} \\ &\quad \times E_{r_0}^{in}(t) \sin(\theta_{p,b,w}^0 + \Omega_p t) \\ &\quad \times e^{j2kz'_{p,b,w} \cos(\theta_{p,b,w}^0 + \Omega_p t)} dz'_{p,b,w} \end{aligned} \quad (2)$$

where  $\eta$  is the intrinsic impedance of air,  $k = 2\pi/\lambda$  is the wave number.  $B$ ,  $W$  and  $P$  are the number of blades per propeller, number of thin wires per blade and number of propellers respectively,  $dz'_{p,b,w}$  is the length of infinitesimal dipole along the  $z$ -axis at the distance  $z_{p,b,w}$  along the  $w^{th}$  wire of the  $b^{th}$  blade of the  $p^{th}$  propeller in the rotation plane.

$r_p$  and  $r_0$  indicate the distance from propeller rotation center and the distance from the drone body to the observation point.  $l_{p,b,w}$  is the length of the  $w^{\text{th}}$  wire of the  $b^{\text{th}}$  blade of the  $p^{\text{th}}$  propeller. The  $p^{\text{th}}$  propeller rotates with the angular velocity  $\Omega_p$  and all angles changes in time linearly:  $\theta_{p,b,w}(t) = \theta_{p,b,w}^0 + \Omega_p t$ , where  $\theta_{p,b,w}^0$  is the initial angle of the  $w^{\text{th}}$  wire of the  $b^{\text{th}}$  blade of the  $p^{\text{th}}$  propeller relatively to the LOS at time  $t = 0$ .  $W$ ,  $\theta_{p,b,w}$  and  $l_{p,b,w}$  depend on the design geometry of propeller.

This synthetic model shows that the frequency of the scattered radio waves depend on the angular velocity of the propellers and time. This is the micro-Doppler effect caused by the rotational motion of the propellers. The micro-Doppler effect induces an additional frequency shift about the main body Doppler frequency [9].

### C. Radio Channel Simulator

The changes from the transmitted signal to the received signal of the antenna result from the scattering by the quadcopter. The radio wave propagation and scattering are collectively given by the radio channel transfer function (CTF).

To obtain the radio CTF, the Ansys HFSS simulator is used. In Ansys HFSS, the shooting and bouncing ray (SBR) technique is chosen for its high frequency electromagnetic solver for modelling EM interaction in electrically large environments. The electrical size, measured in wavelengths, of the drone is approximately  $5.6 \times 5.6 \times 1$  at 5 GHz. HFSS SBR+ computes the performance of antennas, far field radiation patterns and radar signatures for electrically large scenario [12]. SBR+ can be extended with advanced diffraction physics such as PTD and UTD. However, these additional diffraction physics do not play a big role in the scenario (the S-parameters, at several frequency points, has been measured and had a deviation of only 0.3%). Therefore to reduce computation time, no additional simulation extensions are used.

In Ansys HFSS SBR+, the CTF will be computed. The CTF  $\mathbf{H}(f, t) \in \mathbb{C}^{N_r \times N_t}$  is a complex valued matrix consisting of  $N_r$  receiving antenna polarizations and  $N_t$  transmitting antenna polarizations. CTF is a  $2 \times 2$  matrix since this paper focuses on both co- and cross-polarization combinations of transmit-receive antennas. The CTF contains information of the transmitting, propagating, scattering and receiving radio waves in a medium. In Ansys HFSS the simulation environment will be created. This environment is illustrated in Figure 3 and contains:

1) *Two dipole antennas*: Due to the simplification of the realistic dual-dynamics to the single-dynamics, the 'observer' drone is modelled as a transmit and receiver antenna. In order to simulate both co- and cross-polarizations the Tx/Rx antenna consists a set of two identical dipoles mounted at a  $90^\circ$  angle, so the two antenna sets are both horizontally and vertically polarized. The observer drone is assumed to be stationary and the antennas are positioned very close to each other to reduce additional system complexity. The crossed dipole antennas altogether have an omnidirectional radiation pattern, meaning it radiates in every direction, and therefore suitable for radar applications.

2) *Drone*: The scatterer will be modelled as a quadcopter drone in the simulation environment. This drone consists of a body, modelled as a small cuboid, and four equally spaced propellers. The propeller model, which is shown in Fig 2, is imported into HFSS from an online database where users share their CAD models [13].

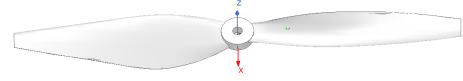


Fig. 2: Imported propeller model

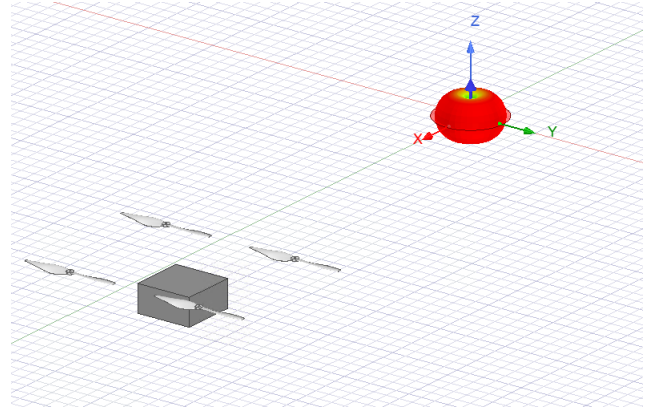


Fig. 3: HFSS simulation setup

### D. Time-frequency transformation

A popular method to extract micro-Doppler signatures from the channel function is the short-time Fourier transform (STFT). The STFT provides the localized time-frequency information of a windowed signal [4]. The STFT of the channel function is given as [11]:

$$\mathbf{H}(\tau, f) = \int_{t_1}^{t_2} \mathbf{H}(t) w(t - \tau) e^{-i2\pi ft} dt \quad (3)$$

where  $\mathbf{H}(t)$  is the channel function at the center frequency,  $w(\tau)$  is window function and  $\tau$  the time-shift of the window.  $t_2 - t_1$  is the time interval at which the STFT is taken and  $f$  is the frequency. From the STFT, a spectrogram can be obtained by taking the magnitude squared of the STFT and by repeatedly increasing  $\tau$ . A spectrogram reveals the spectral content of a time-domain signal and is therefore suitable to detect the micro-Doppler frequencies. To visualize the propeller blade flashes in the spectrogram, a small coherent processing interval (CPI) is needed. For this, we need to choose the processing interval  $N/fs$ , where  $fs$  is the sampling frequency and  $N$  the length of the time window, as a fraction of a full rotation. By applying a long window STFT, multiple propeller rotations are included in the CPI. The spectral content of the spectrogram is now dominated by rotation frequency of the blades, the spectral lines are called HELicopter Rotor Modulation (HERM) lines [17]. In a

long window spectrogram, the HERM lines are separated by  $\Delta f = N_b \Omega_p$  where  $N_b$  is the number of blades per propeller and  $\Omega_p$  is the rotation frequency of the propeller.

From the power spectral density obtained by taking a time slice from the spectrogram, the magnitude of the spectral lines can be seen. Using the rotation frequency of the propellers, the drone orientation can be approximated. This can then be used to make a distinction between the hovering or flying motion of the drone.

### E. Power Delay Profile

In order to detect the range of the drone, it is necessary to compute the time of arrival of the radio signals. There are multiple paths between the transmitter and receiver, caused by the geometry of the drone. To obtain the power of the delayed path components, the power delay profile (PDP) can be utilized. By taking the inverse Fourier transform of the CTF  $\mathbf{H}(f, t) \in \mathbb{C}^{N_r \times N_t}$  the impulse response  $\mathbf{h}(\tau, t) \in \mathbb{C}^{N_r \times N_t}$  can be found. From the impulse response, the PDP can be computed by taking the magnitude squared. The distance from the antenna to the drone can be approximated using the following equation:

$$R = \frac{c_0 \bar{\tau}}{2} \quad (4)$$

where  $c_0$  is the speed of light at which radio waves propagate and  $\bar{\tau}$  is the average delay of the scattered radio waves. To add on that, the detectable delay spread can be used to indicate the size of the drone.

### F. Collision assessment

The strongest spectral peak in the spectrogram corresponds to the velocity of the drone body. When a drone has a relative velocity w.r.t the other drone, it will have a shifted body line in the long window spectrogram. However, knowing the relative velocity between the drones, does not provide full information about the mobility of the other drone.

When using the long window spectrogram, the orientation of the drone can be approximated by looking at power of the spectral peaks. A drone that is coming towards the observer drone is in a pitch motion. The most dominant spectral peaks reveals the rotational velocity of the frontal propellers since the signal strength decreases with distance [14]. The angular velocity of the frontal and rear propellers relates to the pitch angle as described in section II-A.

The delay spread measures differences between the time of arrival of the earliest multipath component and the time of arrival of the last major multipath component. This could be a good indication of the size of the drone.

In order to avoid collisions, the concerned drone has to make sure it can react in a timely manner. According to the paper [15], geofencing can be used to segregate airspace into volumes approved for the use by Unmanned Aerial Systems (UAS). A geofence is a virtual barrier defined by boundaries and can be generated dynamically, e.g. around a moving UAV.

The paper [16] proposed a multi-lane geofencing method. One lane of the air corridor is depicted in Figure 5. The lane

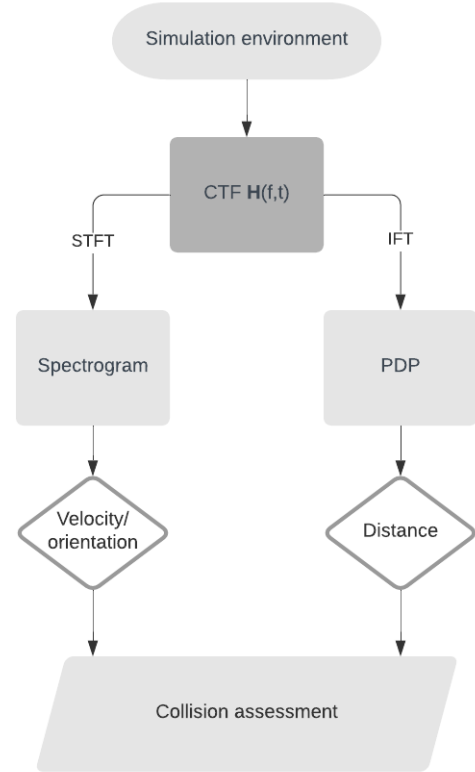


Fig. 4: Methodology overview

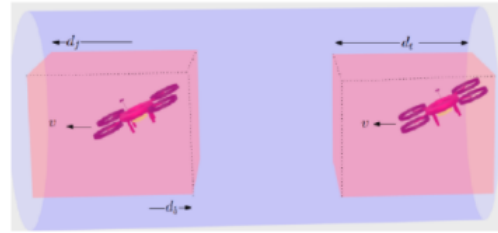


Fig. 5: UAV placement in air corridor [16].

fencing is shown as a cylindrical geofence. In addition, each UAV has a core-geofence which is vital to avoid collisions with other drones. The forward and rear clearances can be governed by the speed of the drone, such that high velocity drones have a larger core-geofence. In case of violating the core-geofence, the observer drone would issue a warning to the other drone to take further actions.

## III. NUMERICAL ANALYSIS

This section presents the system setup, the specifications and the numerical analysis. The full methodology overview, as was introduced in Section II, can be seen in Figure 4. First, the simulation environment needs to be set up. From the simulations the channel transfer function can be obtained. The channel function describes the information of the scattered radio waves. Using the short time Fourier transform and the

inverse Fourier transform, the received power in frequency and delay domain is obtained. From the time-frequency plot, the micro-Doppler signatures can be observed and provides information on the radial velocity of the propeller blades. The delay of the scattered radio waves reveals information about the distance of the target object. Based on this information collision avoidance can be assessed.

#### A. System setup and specifications

In Ansys HFSS, the drone body and propellers are modelled and the dimensions are shown in Table I. The frame size of the drone is defined as the distance between the opposite corner rotors. With 136 mm propellers, the frame size needs to be at least 193 mm, however the frame size is chosen to be 280 mm since the frame size of small to medium sized quadcopter drones is around 300 mm [18].

Parameter	Dimensions [mm]
Drone body	80 x 80 x 40
Propeller	136 x 25 x 1
Frame size	280

TABLE I: Drone dimensions

As explained before, the Tx/Rx antenna will be modelled as a crossed dipole antenna array. A center frequency of 5 GHz, which lies in the C-band, will be used due to the fact that frequencies between 1 to 10 GHz are widely used by air traffic communications, surveillance and weather radar systems [19]. For the power delay profile, we would like a delay resolution such that the individual propellers as well as the drone's body are detected. The distance between propellers and drone body is approximately 80 mm. This means that the delay difference between the scattered radar waves is approximately  $5.3e-10$  seconds. Therefore a bandwidth of 4 GHz is chosen. A bandwidth of 4 GHz will result in a delay resolution of  $\frac{1}{4e9} = 2.5e-10$  seconds, which is a resolution that allows us to view the scattered radio waves of the propellers and body.

Another important design parameter of the pulsed Doppler radar is the pulse repetition frequency (PRF). The PRF is the frequency at which the pulses are emitted, and depends on the range and velocity of the target. According to the Nyquist sampling theory, the sampling frequency needs to be at least twice the maximum frequency of the measured signal [20]. For a Doppler radar, the sampling frequency is the PRF.

The maximum velocity of a propeller is the tip velocity. The tip velocity of a propeller blade rotating at 133 rotations per second with a blade length of 68 mm is approximately 57 m/s. Utilizing equation 1, the maximum Doppler frequency will be approximately 1.9 kHz. The PRF should be at least twice the maximum Doppler frequency and because some drones may have a higher rotation frequency, the PRF is assumed to be 10 kHz. However, a higher PRF will reduce the maximum range it can detect a drone. The maximum range is given by the time it takes for a radiated wave to travel to the target and travel back to the radar system before another pulse has been emitted. For a radar system with a PRF of 10 kHz the maximum range is approximately 15 km which seems to be a suitable range for this application.

The radar specifications are summarized in Table II

Parameter	Value
Tx/Rx antenna type	Cross-polarized dipole
Center frequency [GHz]	5
Bandwidth [GHz]	4
PRF [kHz]	10
Max range [km]	15
Range resolution [mm]	37.5

TABLE II: Radar specifications

In the EM simulator, the quadcopter drone is 'hovering' at 0.5 meters in front of the antenna. For each measurement the propellers are rotated 5 degrees. With a rotational velocity of 8000 rpm, this will result in a radar PRF of approximately 10 kHz. To reduce the computation time in Ansys HFSS, only half a rotation is simulated. Therefore in order to have a difference in angular velocity between the propellers (when in pitch motion for example), the rear motors will rotate twice as fast such that after half a propeller rotation, the propellers are in its original position. The start position of the propellers are perpendicular to the LOS.

#### B. Numerical examples

In total there are 2 x 2 linear polarization pairs of the Tx/Rx antenna. However, for the spectrogram generation only HH-polarization is used since the gain is higher than other polarization pairs. Moreover the micro-doppler signature is more visible in HH-polarization, which makes sense because the propellers are rotating in the horizontal plane. The spectrograms of a drone which is 'flying' in three different motions (pitch angle and propeller configuration are changed) is illustrated in Figure 6. These three motions are 1) Hovering, 2) Pitch motion towards the radar, 3) Pitch motion away from the radar. If the pitch angle of the drone is negative, that means it is flying away from the radar and a positive pitch angle means the drone is flying towards the radar.

The spectrograms are produced using two different window sizes. The short window spectrogram has a time window of 2 ms. This means that the integration interval is small and only a fraction of a full propeller rotation. A small CPI assures that the individual blade flashes are visible on the spectrogram. The long window spectrogram has a time window of 20 ms, meaning that four propeller rotations are included in the CPI. The HERM lines are now visible on the spectrogram.

From the spectrogram, the power spectral density (PSD) is obtained and displayed in Figure 7. Because the long window spectrogram has spectral lines which are constant over time, the PSD is just a time slice of the long window spectrogram.

The PDP is plotted over time and displayed in Figure 8. The top figures are the PDP of a hovering drone, situated at 0.5 m in front of the radar. The bottom two figures show the PDP of a moving drone. In the simulation, the drone moves with a velocity of 10 m/s from 2.5 m to 0.5 m in front of the radar. For the PDP plots, both co- and cross-polarization (HH- and VH-polarization) is shown since there are some noticeable differences in the profile patterns.

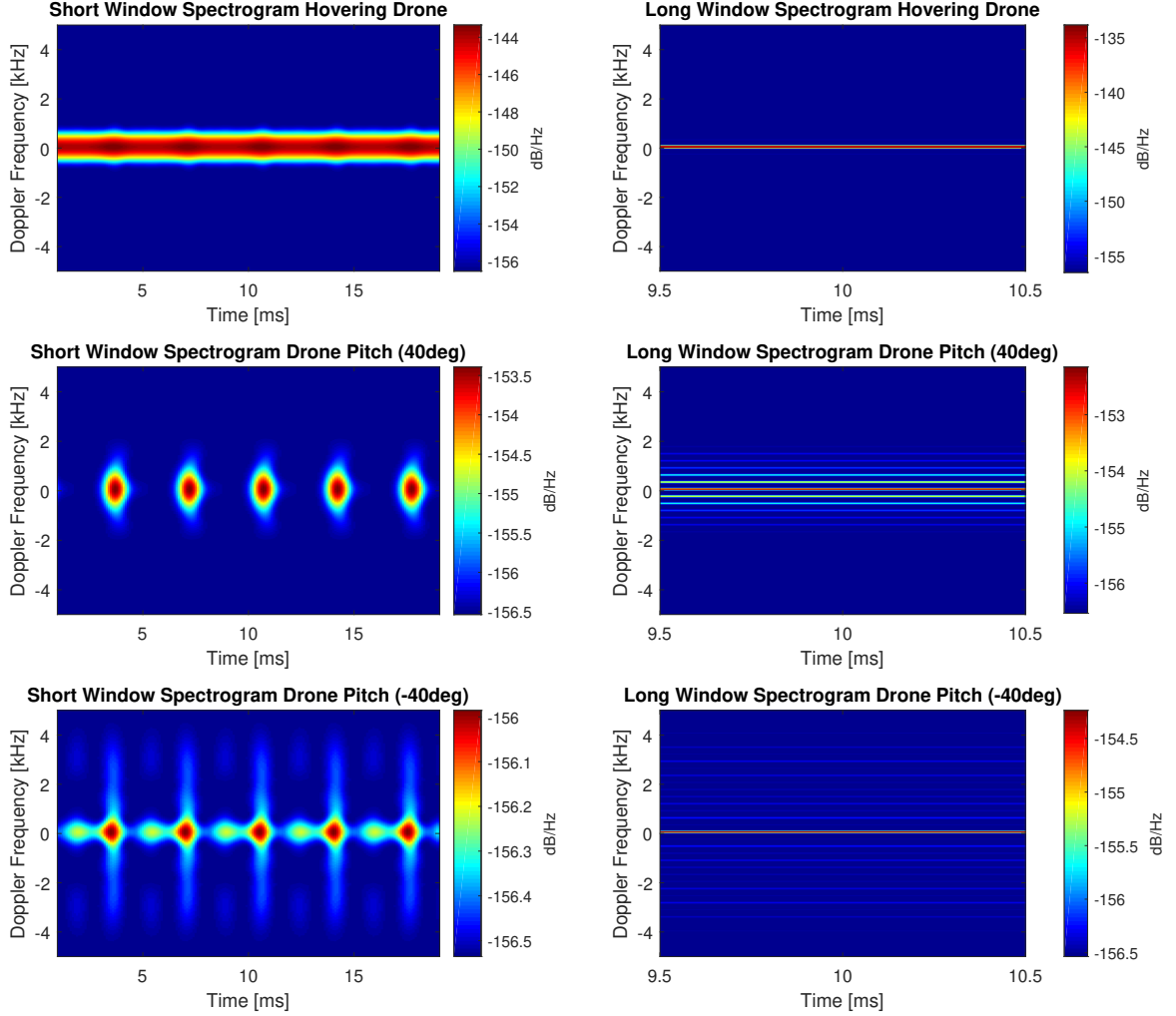


Fig. 6: Spectrogram of a quadcopter drone in 3 positions; hovering, pitch +40deg and pitch -40deg.

### C. Discussion

The spectrograms, seen in Figure 6, for different drone positions, show some clear differences. First of all, a drone hovering does not exert many micro-Doppler signatures. The short window spectrogram gives little information about the angular velocity of the blades. Moreover, the long window spectrogram represents one spectral line, caused by the drone's body. This can be explained by the fact that at the LOS, the propellers are very thin and do not scatter the radio waves as much as the drone body. When the drone is in a forward motion (facing towards the radar), the pitch angle is now at 40 degrees and there is much more radio wave scattering caused by the propellers. In the short window spectrogram, the blade flashes of the frontal rotors (R4 and R3) are seen whereas the rear rotors (R1 and R2), which rotate twice as fast, are not detectable. The spectral peaks, shown in Figure 7, are spaced out by 286 Hz. This value is close to the theoretical spacing of twice the rotation frequency (266Hz). The intensity

of these spectral peaks gradually decrease to a maximum Doppler frequency of  $\pm 2$  kHz. This means that only the frontal propeller rotation frequency is detected. On the contrary, the spectrogram of the quadcopter facing away from the radar has dominant spectral peaks at a frequency spacing of 573 Hz, corresponding to R4 and R3, which are rotating at 266 revolutions per second. The less dominant peaks correspond to R1 and R2 which rotate twice as slow.

The PDP shows the delay of the scattered radio waves of the quadcopter while hovering and moving. Using co-polarization, the drone body is detected, whereas the propellers are not very clear. The average delay is approximately  $3.75e-9$  seconds which coincides to a range of 0.56 m. When the measurement of cross-polarized antenna's are used, the propellers are detected instead of the drone body. This can be due to the fact that a propeller is very thin compared to the wavelength of the incoming radio waves. The vertically polarised waves then change direction because of diffraction.

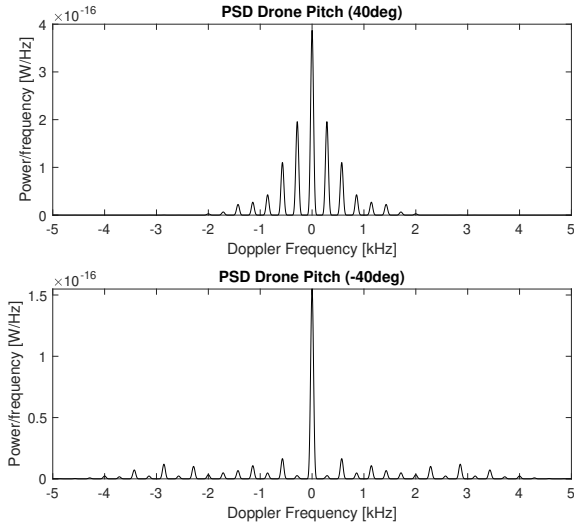


Fig. 7: PSD of the radar pulses scattered on a quadcopter for different drone pitch angles (+40deg).

This is also called knife-edge-diffraction and causes more scattering of unpolarized radio waves. It should be noted that this phenomenon is mostly observable when the Tx/Rx antenna is VH polarized because the received power with HV-polarization antennas is approximately 15dB lower.

#### D. Collision avoidance

This section will explain how the obtained spectrograms and power delay profiles relate to a collision scheme in air corridor. First of all, when a drone is hovering in LOS w.r.t the observer, there are no micro-Doppler signatures visible on the spectrogram. Moreover, the distance to the hovering drone as well as the drone size can be observed. The individual blades of the propeller are observable on the PDP when using the antennas VH-polarization setup (Figure 8). The observer drone can plan its trajectory based on that information.

Another situation might be that a drone is flying towards the observer. The relative velocity is observed by looking at the Doppler frequency of the UAV bodyframe, which corresponds to the largest spectral peak. The sidelobes on the PSD plot (Figure 7) shows the micro-Doppler signatures and provides information about in which direction the target drone is flying. Moreover, Figure 7 shows that if the targeted drone is facing towards the observer, the spectral peaks are relatively large compared to the body line and the first spectral peak is at the frequency of two times the propeller rotation frequency of the frontal propellers. The rear propeller rotation frequency is however not detectable. In order to avoid the collision, the observer drone has to plan out a trajectory.

There might be a situation where both drones fly in the same direction but the observer drone has a higher velocity than the target drone. Figure 7 shows that the observer can notice the target drone having a negative pitch angle. To avoid a collision the target drone can reduce its speed such that it does not crash into the other drone.

## IV. CONCLUSION

The objective of this paper is to detect the air mobility of a rotary drone by exploiting the backscattering dominated radio channel properties in order to avoid UAV collisions in air corridor. In the simulation setups, a pair of cross-polarized antennas are assumed to be mounted on the observer drone to transmit and receive radio signals. The observer drone detects the air mobility of a target drone. The assumption made here is that the dual-dynamics is simplified into single-dynamics, hence the relative mobility is estimated. I also assumed that the observer drone body does not influence the antenna properties.

From the numerical analysis in Section III, I come to the following conclusions.

- 1) When the transmit-receive antenna are co-polarized, the angular velocity of the propellers can be retrieved from the long window spectrogram.
- 2) The magnitude of the spectral lines in the long window spectrogram reveals information about the pitch angle of the drone.
- 3) When the transmit-receive antenna are VH-polarized, the distance of the propellers, w.r.t the observer, can be observed.

For future work, the micro-Doppler signatures can be further processed enabling classification algorithms to make a quick distinction between the different motions of the drone. Moreover, since this paper was EM simulator based, one could further research this topic in a real-world setting, taking into account the dual-dynamics as well as the influences of both UAVs' body frames on air-to-air radio channel.

## ACKNOWLEDGEMENT

I would like to thank my supervisor dr. Y. Miao for her guidance and assistance throughout the project. Furthermore, I would like to thank MSc. H. Alidoustaghdam for providing me with his assistance and the EM simulation software.

## REFERENCES

- [1] L. Gipson, *Advanced Air Mobility National Campaign Overview*, NASA AAM National Campaign, Mar. 2020. Accessed on: Jun. 23, 2021. [Online]. Available: <https://www.nasa.gov/aeroresearch/aam/description/>
- [2] A. Chapman, *Drone Types: Multi-Rotor vs Fixed-Wing vs Single Rotor vs Hybrid Vtol*, Australian DRONE, Jun. 3, 2016. Accessed on: Jun. 23, 2021. [Online]. Available: <https://www.auav.com.au/articles/drone-types/>
- [3] Cai, Y., Krasnov, O., & Yarovoy, A. (2019). Radar Recognition of Multi-Propeller Drones using MicroDoppler Linear Spectra. In *EuRAD 2019 - 2019 16th European Radar Conference* (pp. 185 – 188). [8904765] (EuRAD 2019 - 2019 16th European Radar Conference). EuMA.
- [4] R. I. A. Harmanny, J. J. M. de Wit and G. P. Cabic, "Radar micro-Doppler feature extraction using the spectrogram and the cepstrogram," 2014 11th European Radar Conference, 2014, pp. 165-168, doi: 10.1109/EuRAD.2014.6991233.
- [5] R. Allain, *How Do Drones Fly? Physics, of Course!*, WIRED, May. 19, 2017. Accessed on: Jun. 21, 2021. [Online]. Available: <https://www.wired.com/2017/05/the-physics-of-drones/>
- [6] T. Townrow, *Drone Series: Do The Risks of Drones Outweigh The Rewards?*, International Airport Review, Mar. 6, 2019. Accessed on: Jun. 21, 2021. [Online]. Available: <https://www.internationalairportreview.com/article/81934/drone-series-risk-reward/>
- [7] *Phantom 4 Specs*, DJI, Accessed on: Jun. 22, 2021. [Online]. Available: <https://www.dji.com/nl/phantom-4/info>
- [8] Hordijk, Bas & Scheper, Kirk Croon, Guido. (2018). Vertical Landing for Micro Air Vehicles using Event-Based Optical Flow. *Journal of Field Robotics*. 35. 69-90. 10.1002/rob.21764.

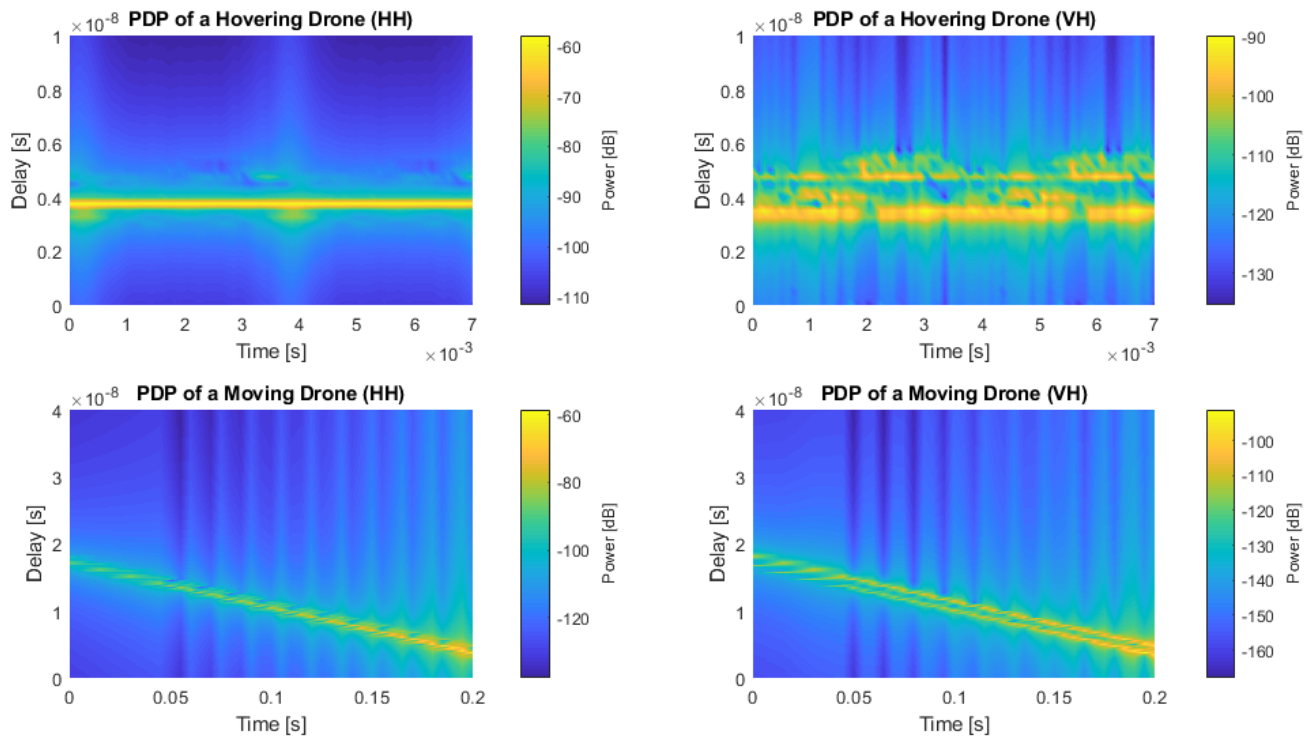


Fig. 8: PDP of a hovering and moving drone for HH- and VH-polarization

- [9] V. C. Chen, F. Li, S. - Ho and H. Wechsler, "Micro-Doppler effect in radar: phenomenon, model, and simulation study," in IEEE Transactions on Aerospace and Electronic Systems, vol. 42, no. 1, pp. 2-21, Jan. 2006, doi: 10.1109/TAES.2006.1603402.
- [10] Y. Cai, O. Krasnov and A. Yarovoy, "Simulation of Radar Micro-Doppler Patterns for Multi-Propeller Drones," 2019 International Radar Conference (RADAR), 2019, pp. 1-5, doi: 10.1109/RADAR41533.2019.171372.
- [11] *Short-time Fourier transform*, Wikipedia, Wikimedia Foundation, Accessed on: Jun. 25, 2021. [Online]. Available: [https://nl.wikipedia.org/wiki/Short-time\\_Fourier\\_transform](https://nl.wikipedia.org/wiki/Short-time_Fourier_transform)
- [12] *Ansys HFSS SBR+*, ANSYS, Inc., 2021, Accessed on: Jun. 22, 2021. [Online]. Available: <https://www.ansys.com/content/dam/product/electronics/hfss/ansys-sbr-plus.pdf>
- [13] S. Suprayitno, *Propeller Blade*, Grabcad, May. 9, 2021. Accessed on: May. 31, 2021. [Online]. Available: <https://grabcad.com/library/propeller-blade-21>
- [14] *Friis transmission equation*, Wikipedia, Wikimedia Foundation, Accessed on: Jun. 24, 2021. [Online]. Available: [https://en.wikipedia.org/wiki/Friis\\_transmission\\_equation](https://en.wikipedia.org/wiki/Friis_transmission_equation)
- [15] Stevens, Mia N., and Ella M. Atkins. *Geofencing in Immediate Reaches Airspace for Unmanned Aircraft System Traffic Management*. 2018 AIAA Information Systems-AIAA Infotech@ Aerospace. 2018. 2140.
- [16] Tony, Lima Ratnoo, Ashwini Ghose, Debasish. (2020). *CORRIDRONE: Corridors for Drones, An Adaptive On-Demand Multi-Lane Design and Testbed*.
- [17] Klaer, P.; Huang, A.; Sévigny, P.; Rajan, S.; Pant, S.; Patnaik, P.; Balaji, B. An Investigation of Rotary Drone HERM Line Spectrum under Manoeuvring Conditions. *Sensors* 2020, 20, 5940. <https://doi.org/10.3390/s20205940>
- [18] Eric, *Drone (Quadcopter) Frame Sizes - Mini, Micro, Nano*, Learning RC, May 11, 2017. Accessed on: Jun. 18, 2021. [Online]. Available: <http://learningrc.com/drone-quadcopter-frame-sizes/>
- [19] Federal Aviation Administration *Spectrum Engineering & Policy - Radio Frequency Bands Supporting Aviation*, Accessed on: May 11, 2021. [Online]. Available: [https://www.faa.gov/about/office\\_org/headquarters\\_offices/ato/service\\_units/techops/safety\\_ops\\_support/spec\\_management/engineering\\_office/rfb.cfm](https://www.faa.gov/about/office_org/headquarters_offices/ato/service_units/techops/safety_ops_support/spec_management/engineering_office/rfb.cfm)
- [20] B. Karlsson, *Modeling Multicopter radar return: A study in discrimination of multicopter UAVs from birds*, Master's thesis in Applied Physics: Chalmers University of Technology, 2017, pp.1-55.